Bone 120 (2019) 114–124

Contents lists available at ScienceDirect

Bone

journal homepage: www.elsevier.com/locate/bone

Full Length Article

Systemic bone loss, impaired osteogenic activity and type I muscle fiber atrophy in mice with elastase-induced pulmonary emphysema: Establishment of a COPD-related osteoporosis mouse model

Manabu Tsukamoto[a,*,1], Toshiharu Mori[b], Ke-Yong Wang[c], Yasuaki Okada[a], Hokuto Fukuda[a], Keisuke Naito[d], Yoshiaki Yamanaka[a], Ken Sabanai[a], Eiichiro Nakamura[a], Kazuhiro Yatera[d], Akinori Sakai[a]

[a] Department of Orthopaedic Surgery, School of Medicine, University of Occupational and Environmental Health, 1-1 Iseigaoka, Yahatanishi-ku, Kitakyushu 807-8555, Japan
[b] Department of Orthopaedic Surgery, Shin-Kokura Hospital, Federation of National Public Service, Personnel Mutual Aid Associations, 1-3-1 Kanada, Kokurakita-ku, Kitakyushu 803-8505, Japan
[c] Shared-Use Research Center, School of Medicine, University of Occupational and Environmental Health, 1-1 Iseigaoka, Yahatanishi-ku, Kitakyushu 807-8555, Japan
[d] Department of Respiratory Medicine, School of Medicine, University of Occupational and Environmental Health, 1-1 Iseigaoka, Yahatanishi-ku, Kitakyushu 807-8555, Japan

ARTICLE INFO

Keywords:
Chronic obstructive pulmonary disease
Histomorphometry
Bone formation
Slow twitch
Muscle wasting

ABSTRACT

Although it is suggested that chronic obstructive pulmonary disease (COPD) and bone are related, almost all of the pathological mechanisms of COPD-related osteoporosis remain unknown. There is a mouse model showing a deterioration of bone quality after cigarette smoke exposure; however, in smoking exposure models, various factors exist that affect bone metabolism, such as smoking and body weight loss (muscle and fat mass loss). We considered it appropriate to use an elastase-induced emphysema model to exclude factors influencing bone metabolism and to investigate the influence of pulmonary emphysema on bone metabolism. The purpose of this study was to establish a COPD/emphysema-related osteoporosis mouse model by using the elastase-induced emphysema model. The lumbar vertebrae and femurs/tibiae exhibited trabecular bone loss and impaired osteogenic activity in 24-week-old male elastase-induced emphysema model mice. In addition, the model mice showed atrophy of type I muscle fibers without atrophy of type II muscle fibers. We believe that the mice described in this experimental protocol will be accepted as a COPD/emphysema-related osteoporosis mouse model and contribute to further investigations.

1. Introduction

Chronic obstructive pulmonary disease (COPD) demonstrates skeletal muscle and bone disorders as extrapulmonary lesions and is a risk factor for osteoporosis and sarcopenia [1–8]. Patients diagnosed with COPD have a high prevalence of osteoporosis [9]. The prevalence of vertebral fractures in COPD patients is 24 to 63% [10], and thoracic vertebral fractures occur more often than lumbar vertebral fractures [11]. In addition, COPD is the most frequent disease as a cause of secondary osteoporosis in men [12].

Chronic inflammation due to many factors occurs in the lungs of patients with COPD, and irreversible loss of alveolar surface and depletion of lung elastin, which are pulmonary emphysema findings, have been identified [13]. There is also a clinical phenotype called combined pulmonary fibrosis and emphysema (CPFE), which is characterized by the coexistence of pulmonary fibrosis and emphysema [14], but emphysema volume has especially been shown to be strongly related to vertebral bone mineral density (BMD) [15]. Almost all of the pathological mechanisms of COPD/emphysema-related osteoporosis remain unknown, although it is suggested that COPD/emphysema is related to bone.

The problem in investigating the pathological mechanism of COPD-related osteoporosis is that various factors exist that affect bone metabolism, such as smoking [16], body weight [17], COPD exacerbation

* Corresponding author at: 1-1 Iseigaoka, Yahatanishi-ku, Kitakyushu 807-8555, Japan.
E-mail address: m-tsuka@med.uoeh-u.ac.jp (M. Tsukamoto).
[1] Present/permanent address: Department of Orthopaedic Surgery, School of Medicine, University of Occupational and Environmental Health, 1-1 Iseigaoka, Yahatanishi-ku, Kitakyushu, 807-8555, Japan.

https://doi.org/10.1016/j.bone.2018.10.017
Received 2 July 2018; Received in revised form 16 October 2018; Accepted 16 October 2018
Available online 17 October 2018

[18], use of steroids [19], and sarcopenia [20]. In particular, sarcopenia and body weight loss in COPD subjects are related to excessive energy expenditure by respiratory muscles, systemic inflammation, nutrition disability and physical inactivity. Analysis excluding these factors is difficult in humans, and analysis in an animal model is desired; however, there is currently an absence of an appropriate animal model for COPD/emphysema-related osteoporosis patients.

Several pulmonary emphysema models exist [21], such as smoking exposure models, transgenic animals, and elastase-induced emphysema models. The smoking exposure model is the one most commonly used as a COPD animal model, and it demonstrates the deterioration of bone quality [22]. However, there is no unified experimental protocol [23]. In addition, the degree of emphysema is mild; therefore, it may be the influence of smoking exposure rather than emphysema causing bone to degrade. Problematically, not only weight but also fat and muscle mass decrease systemically over time [24]. In transgenic animals, we must consider the effect of genetic modifications on bone. An elastase-induced emphysema model is used to initiate the inflammatory response seen in COPD and to induce an inflammatory response to make it permanent [23]. The greatest advantage is that we can control the severity of pulmonary emphysema depending on the elastase dosage. Therefore, we considered it appropriate to use this model to exclude factors influencing bone metabolism (smoking, body weight loss, muscle mass loss) and to investigate the influence of COPD/emphysema on bone metabolism.

It is necessary for us develop a mouse model to elucidate the pathological mechanisms of a COPD/emphysema-related osteoporosis. We planned the following study, utilizing the elastase-induced emphysema model to establish an appropriate animal model for patients with COPD/emphysema-related osteoporosis. The purposes of our study are 1) to verify the elastase dosage that induces the emphysema without complications (weakness and body weight loss) and 2) to evaluate the bones and muscles of the pulmonary emphysema model mice. In addition, this study establishes a mouse model of patients with COPD/emphysema-related osteoporosis.

2. Materials and methods

2.1. Mice

The experimental protocol was approved by the Ethics Review Committee for Animal Experimentation of the University of Occupational and Environmental Health (approval number, AE11-014). A total of 56 eight-week-old male C57BL/6 J mice (approximately 20 g) were purchased from Charles River Japan (Tokyo, Japan) and acclimated for 4 weeks under standard laboratory conditions (temperature 24 ± 1 °C, humidity 55 ± 5%). All of the mice were housed in similarly designed cages. The light/dark cycle was 12 h, with lights on from 7:00 a.m. to 7:00 p.m. Drinking water and food were available ad libitum. All of the mice were fed a commercial mouse diet (CE-2; Japan CLEA, Tokyo, Japan) containing 1.25% calcium and 1.06% phosphorus.

2.2. Experimental protocol

The experimental protocol design is shown in Fig. 1A. Mice aged 12 weeks (24–27 g) were anesthetized by an intraperitoneal injection of 0.3 mg/kg of medetomidine (Kyoritsu Seiyaku Corporation, Tokyo, Japan), 1.0 mg/kg of midazolam (Astellas Pharma Inc., Tokyo, Japan), and 5.0 mg/kg of butorphanol (Meiji Seika Pharma Co., Ltd., Tokyo, Japan), followed by the intratracheal administration of 0.025 U, 0.1 U, or 0.25 U porcine pancreatic elastase (PPE: Sigma-Aldrich Inc., St. Louis, MO) dissolved in 50 ml of saline (the PPE 0.025, PPE 0.1 and PPE 0.25 groups, respectively) or 50 ml of saline alone (the Control group) into the trachea [25–28]. The administration of PPE into both lungs of all mice was confirmed by a microcomputed tomography (μCT). The body weight of the mice in each group was measured every week. At week 12, the 24-week-old mice were sacrificed, and blood samples, the spine, the bilateral lungs, femurs, tibias, and leg muscles were obtained for analysis. The bone and muscle data of the group without complications (weakness or body weight loss) was compared with the data of the Control group.

2.3. Lung histomorphometry

Lungs were inflated with 0.1 M phosphate-buffered saline (PBS) at a pressure of 25 cm H_2O and then fixed with 4% paraformaldehyde (PFA) in 0.1 M PBS. After paraffin embedding, the lung tissue was cut in 5-μm thick slices and stained with hematoxylin and eosin (H&E). The H&E-stained sections were evaluated under a microscope using an image analysis measurement system (WinROOF 2015, MITANI Corporation, Tokyo, Japan). The mean linear intercept (Lm), an indicator of the mean alveolar diameter [29], was assessed in 20 randomly selected fields of the left lung parenchyma at 100 × magnification, and the images were manually thresholded. The airway and vascular structures were eliminated from the analysis.

2.4. Dual-energy X-ray absorption

The spine (T3-L5) and left femur of 24-week-old mice were prepared by removing all of the soft tissue, and then the BMD (mg/cm^2) was measured with DXA (DCS-600, Aloka, Tokyo, Japan) [30–32].

2.5. Microstructural analysis of trabecular bone using microcomputed tomography

Using in vivo μCT imaging (CosmoScan GX; Rigaku, Tokyo, Japan), changes in the BMD of vertebrae (T4, T7, T10, L1, and L4) were tracked over 12 weeks. All of the mice were scanned with the μCT at weeks 0, 4, 8, and 12 (90 kVp, 88 μA, 142.86-ms integration time, and a resolution of 18 × 18 × 18 μm^3 after reconstruction), and the total BMD, including the trabeculae and cortex, of each vertebra was analyzed using BMD measurement software (BoneAnalysis, Rigaku Corporation, Tokyo, Japan).

The trabecular bones of the first lumbar vertebra (L1) and left distal femoral metaphysis obtained at week 12 were analyzed by a μCT system with a resolution of 10 × 10 × 10 μm^3 (90 kVp, 88 μA, 533.33-ms integration time) in a vertebral or metaphyseal volume of interest (VOI) with a height of a 1.0 mm, commencing 0.5 mm proximal to the growth plate. The filter type was median (Kernel size; 5 × 5 × 5). The minimum threshold for bone density was 334 mg/cm^3 determined through correlation to phantoms of known density [33]. The bone microstructure parameters in the trabecular bone of L1 and the distal femoral metaphysis were evaluated using Analyze 12.0 software (AnalyzeDirect, Inc., KS, USA) and presented as follows: trabecular bone volume (BV/TV: %), trabecular thickness (Tb.Th: mm), trabecular separation (Tb.Sp: mm), trabecular number (Tb.N: 1/mm), structure model index (SMI), and connectivity density (Conn.D: 1/mm^3) [34].

2.6. Static and dynamic bone histomorphometry in nondecalcified specimens

Bone histomorphometry was performed using nondecalcified specimens as previously described [31,32]. The lumbar vertebrae (L1–4) and right proximal tibiae were embedded in methyl methacrylate (MMA) after Villanueva's bone staining. Five-μm-thick sagittal (lumbar vertebrae) or coronal (tibiae) sections of nondecalcified specimens were cut on a microtome. Histomorphometry was performed using a semi-automatic image analysis system linked to a light microscope (Histometry-RT, SYSTEM SUPPLY, Nagano, Japan). The secondary spongiosa area was determined for each section. To exclude the primary spongiosa, the regions within 250 μm of the growth plate and one cortical shell-width of the endocortical surface were not measured. Regarding

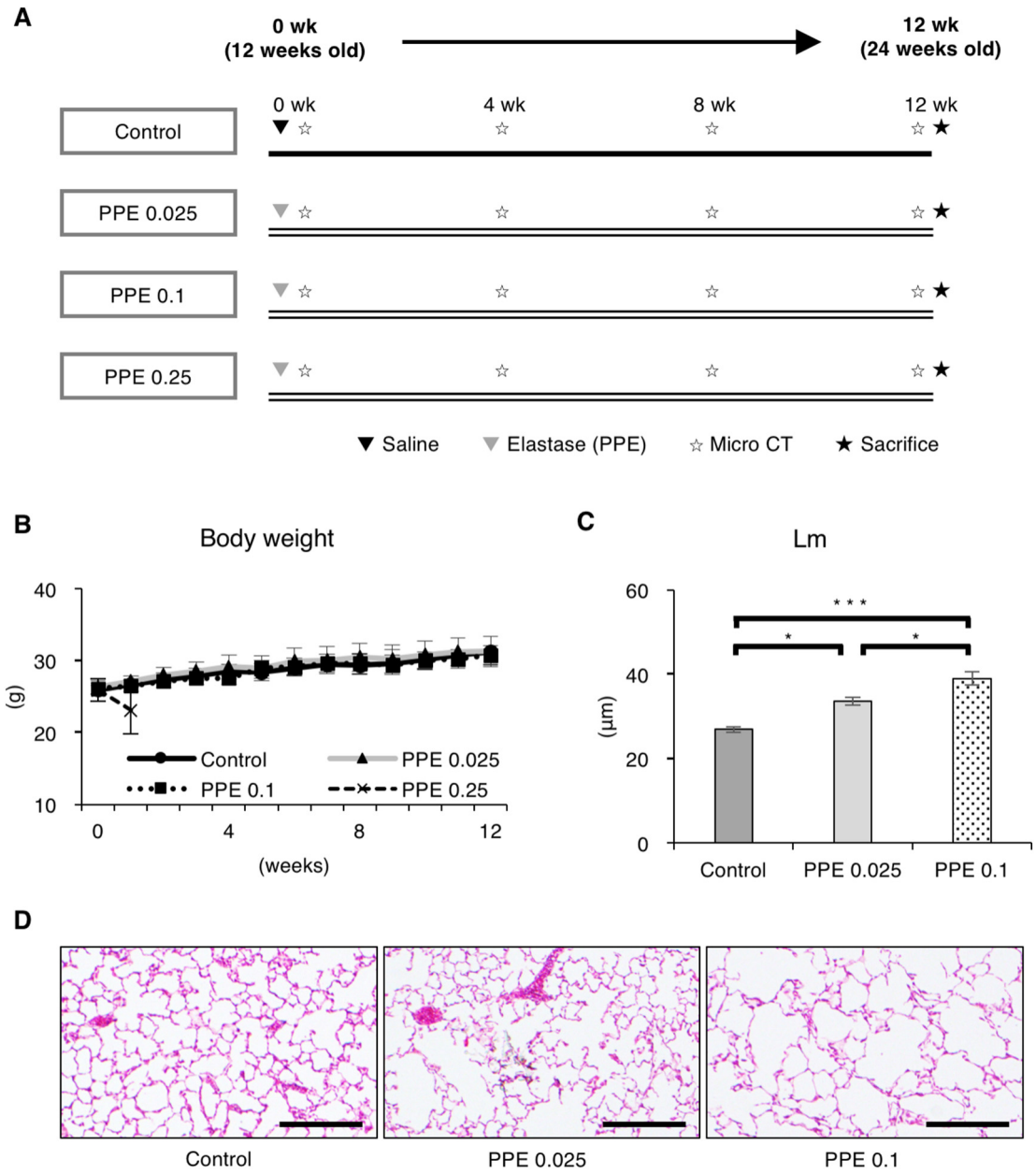

Fig. 1. Experimental protocol, body weights, and lung morphometric analysis in each group.
(A) Experimental protocol. (B) The sequential changes in body weight. Data are the mean ± SD (n = 7 in each group). (C) The mean linear intercept (Lm) values as a parameter of emphysema. Data are the mean ± SE (n = 14 in each group). *p < 0.05, ***p < 0.001. (D) Representative images of H&E-stained lung sections at week 12 after saline or elastase administration stained with hematoxylin and eosin. Scale bar = 200 μm.

the structural parameters, the BV/TV (%), the osteoid surface (OS/BS: %) and the osteoblast surface (Ob.S/BS: %) were determined, and the mineralizing surface (MS/BS: %), the mineral apposition rate (MAR: μm/day) and the surface referent bone formation rate (BFR/BS: mm^3/mm^2/year) were obtained using luminescence microscopy, as reported previously [35]. Regarding the bone resorption parameters, the osteoclast surface (Oc.S/BS: %) was measured in the right proximal tibia. The cells that formed resorption lacunae on the surface of the trabeculae and contained two or more nuclei were identified as osteoclasts [32]. The abbreviations for the histomorphometric parameters were derived from the recommendations of the Histomorphometry Nomenclature Committee of the American Society for Bone and Mineral Research [35,36].

2.7. Systemic bone chemical markers

Blood samples were collected from anesthetized mice via a retro-orbital bleed at 12 weeks. The plasma was obtained by centrifugation, and the samples were stored at −30 °C until testing. The plasma level of osteocalcin was determined using an enzyme immunoassay (EIA) kit (Mouse Gla-Osteocalcin High Sensitive EIA Kit, Takara Bio, Shiga, Japan), and the plasma level of tartrate-resistant acid phosphatase-5b (TRACP-5b) was examined using an enzyme-linked immunosorbent assay (ELISA) kit (MouseTRAP™ Assay, Immunodiagnostic Systems, Fountain Hills, Maricopa Country, Arizona, USA).

2.8. Muscle mass

The left quadriceps, gastrocnemius, plantaris, and soleus muscles

were removed, cleaned of extraneous tissue, and weighed during necropsy. Absolute measurements were normalized to the total body weights of each mouse.

2.9. Cross-sectional myofiber measurements

The muscles were then placed in 4% PFA for 24 h and transferred to 70% ethanol for future staining with H&E for morphologic evaluation. The right-sided gastrocnemius and soleus muscles were transversely sectioned at the middle of the muscle belly and then sectioned at 5-μm and stained with H&E. An average of 300 myofibers were evaluated for morphology, and the myofiber cross-sectional area (CSA) was determined using ImageJ software (NIH) [37].

2.10. Immunofluorescence staining of muscular fibers

Right quadriceps muscles were embedded in O.C.T. Compound (Sakura Finetek Japan Co., Ltd., Tokyo, Japan) and then sectioned at 5 μm. The frozen sections of quadriceps muscles were rinsed with PBS and immediately fixed in 4% PFA in 0.1 M PBS for 15 min. For the permeabilization step, we covered tissue sections with ice-cold 100% methanol and incubated the tissue in methanol for 10 min at −20 °C. A blocking step was performed to reduce nonspecific staining by immersing the slides in 1% BSA/5% normal goat serum for 60 min.

Type I (slow twitch) and type II (fast twitch) are included in muscle fibers, and type II is divided into three subtypes (IIA, IID/X, and IIB). Immunofluorescence staining of type I muscle fibers (BA-F8 primary antibody, DSHB, dilution 1:100), type IIA muscle fibers (SC-71 primary antibody, DSHB, dilution 1:200), type IID/X muscle fibers (6H1 primary antibody, DSHB, dilution 1:20) and type IIB muscle fibers (BF-F3 primary antibody, DSHB, dilution 1:100) was then conducted. For double-immunofluorescence staining (I & IIA, I & IID/X, I & IIB), the frozen sections were labeled with mouse monoclonal BA-F8 and mouse monoclonal SC-71, 6H1 or BF-F3 antibodies and then visualized with goat antimouse IgG antibodies conjugated with Alexa Fluor dyes (*red-stained*, Thermo Fisher, dilution 1:200) and goat antimouse IgM antibodies conjugated with Alexa Fluor dyes (*green-stained*, Thermo Fisher, dilution 1:200).

2.11. Measurement of the type I muscle fiber area

Most type I muscle fibers are contained in the intermediate vastus in mice, whereas few are contained in the vastus lateralis. Thus, a region of interest (ROI) in the intermediate vastus was determined for each section because type I muscle fibers are abundant in this region. The area of ROI was 320,000 μm^2 (400 μm × 800 μm) except for measurements of the width of one fiber from the muscular membrane of the rectus femoris and vastus medialis (the muscular membrane between intermediate vastus and vastus lateralis is unclear). We analyzed the proportion of each muscle fiber (type I, type IIA, type IID/X, and type IIB) within the ROI.

2.12. Statistical analysis

The data are shown as the mean ± SD or SE. Body weight was analyzed using repeated measures ANOVA, and Lm was analyzed using one-way ANOVA with Tukey's post hoc test. Compared with the Control group, the influence of pulmonary emphysema on the change rates of BMD at each vertebra (T4, T7, T10, L1, and L4) was computed by repeated measures ANOVA. One-way ANOVA with Bonferroni's post hoc test was used to detect differences between the potential effects of the Control, PPE 0.025 and PPE 0.1 groups. Differences were considered significant at $p < 0.05$. All statistical analyses were performed with STATA/IC 14 (StataCorp, College Station, TX, USA) on a Macintosh computer.

3. Results

3.1. Body weight

The experimental protocol design is shown in Fig. 1A. Seven of the 14 mice in the PPE 0.25 group were euthanized after a few days due to weakness. Four of the remaining 7 mice showed body weight losses of 15% or more at day 7 after intratracheal administration; thus, the experiment was stopped for the PPE 0.25 group. There were no significant differences in body weight at each week among the Control, PPE 0.025, and PPE 0.1 groups (Fig. 1B).

3.2. Lung histomorphometry

The effect of PPE administration into the trachea on pulmonary alveoli was dose dependent. The mean value of the linear intercept in lung specimens in the PPE 0.025 group was significantly higher than that in the Control group, and the value in the PPE 0.1 group was much higher (Fig. 1C–D).

3.3. Sequential changes in bone mineral density

The rates of change in the BMD of each vertebra (T4, T7, T10, L1, and L4) scanned by μCT are shown in Fig. 2. No significant difference in the BMD change rates was found between baseline and week 12 in the Control group, but the BMD change rate at week 12 in the PPE 0.025 (T10 and L4) and PPE 0.1 groups (T4, T7, T10, L1 and L4) was significantly lower than that at baseline. Regarding all vertebrae, the change rates of BMD at 4, 8, and 12 weeks after intratracheal administration in the PPE 0.1 group were significantly lower than those in the Control group (Fig. 2A–E). In addition, the change rate of BMD at 12 weeks in the PPE 0.025 group was significantly lower than that in the Control group, and the value in the PPE 0.1 group was much lower. Finally, significant differences were observed in the BMD of the extracted spine (T3–L5), as measured by DXA, between the Control and PPE 0.1 groups at week 12 (Fig. 2F).

3.4. Microstructural analysis using microcomputed tomography

μCT imaging showed a significant difference in L1 trabecular bone (Fig. 3A). Regarding the microstructural parameters of the trabecular bone at L1, significantly lower values for the BV/TV were observed in the PPE 0.1 group than in the Control group. The value of Tb.Sp in the PPE 0.1 group was significantly higher than that in the Control group. Significant differences in Tb.Th, Tb.N, SMI, or Conn.D were not observed (Fig. 3B–G). Lm showed a strong correlation with BV/TV at L1 (Fig. 3H).

Trabecular bone imaging of the femur using μCT also showed a significant difference (Fig. 3I). Regarding the microstructural parameters of the trabecular bone at the distal femur, the values of BV/TV, Tb.N, and Conn.D in the PPE 0.1 group were significantly lower than those in the Control group, and the value of Tb.Sp in the PPE group was significantly higher than that in the Control group (Fig. 3J–O). Lm showed a moderate correlation with BV/TV at the distal femur (Fig. 3P).

3.5. Analysis of static and dynamic histomorphometry

Regarding static and dynamic bone histomorphometry of the trabecular bone at L1–4, significantly lower values for BV/TV and OS/BS were observed in the PPE 0.1 group than in the Control group, and significantly lower values for MS/BS, MAR and BFR/BS were observed in the PPE 0.025 and PPE 0.1 groups than in the Control group. In addition, the value of MAR in the PPE 0.1 group was significantly lower than that in PPE 0.025 group. Significant differences in the Oc.S/BS or the Ob.S/BS were not observed among all groups (Fig. 4A–H).

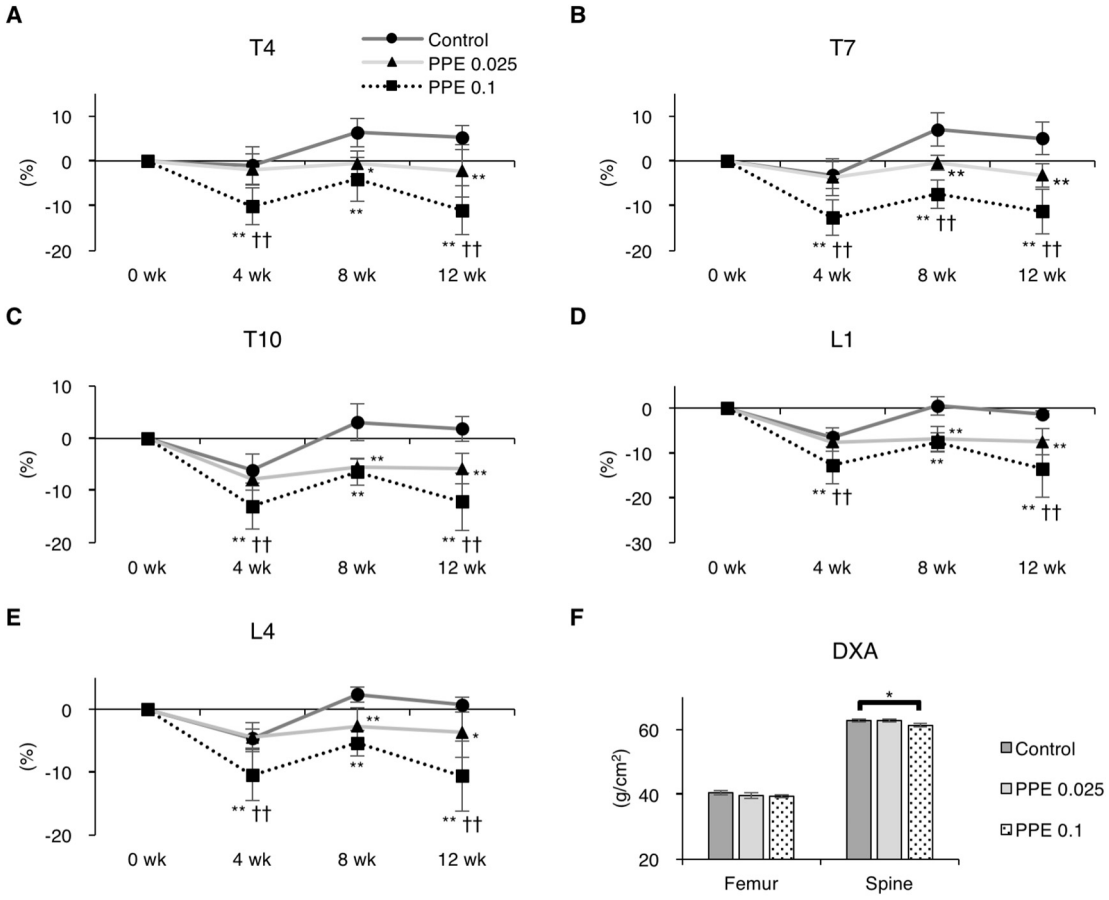

Fig. 2. Bone mineral density of each vertebra.
(A–E) The sequential changes in BMD at each vertebra. Data are the mean ± SD (n = 7 in each group). The asterisks indicate a significant difference from the age-matched Control group value; *p < 0.05, **p < 0.01. The daggers indicate a significant difference from the age-matched PPE 0.025 group value; ††p < 0.01. (F) The BMD of spines and femurs measured by DXA. Data are the mean ± SE (n = 14 in each group). *p < 0.05.

Regarding static and dynamic bone histomorphometry of trabecular bone also at the proximal tibiae, the values of BV/TV and OS/BS in the PPE 0.1 group were significantly lower than those in the Control group. Significantly lower values for MS/BS, MAR, and BFR/BS were observed in the PPE 0.025 and PPE 0.1 groups than in the Control group. There were no significant differences in Oc.S/BS or Ob.S/BS between the PPE 0.1 and Control groups (Fig. 5A–H).

3.6. Systemic chemical markers of bone metabolism

The plasma level of osteocalcin in the PPE 0.1 group was significantly lower than that in the Control group (Fig. 6A). However, there was no significant difference in the plasma level of TRACP-5b among all of the groups (Fig. 6B).

3.7. Muscle mass of the lower limbs and the proportion of type I muscle fibers in the intermediate vastus

There were no significant differences in the weights of the quadriceps, gastrocnemius or plantaris among all of the groups (Fig. 7A–C). Only the soleus weight in the PPE 0.025 and PPE 0.1 groups was significantly less than that in the Control group (Fig. 7D). Similarly, no significant differences were shown in the quadriceps, gastrocnemius or plantaris muscle masses normalized to body weight among all of the groups, and the soleus muscle mass normalized to body weight in the PPE 0.1 group was significantly less than that in the Control group (Fig. 7E–H). The soleus muscle fibers of PPE 0.1 group appear to be atrophied (Fig. 7I). A significant difference in the CSA of 300 muscle fibers in the gastrocnemius was not observed among all of the groups. However, the CSA of 300 muscle fibers in the soleus was significantly lower than that in the Control group (Fig. 7J). Thus, it was suggested that the area per fiber is small and that the diameter of the muscle fiber is short.

We analyzed the proportion of type I muscle fibers in the ROI determined in the intermediate vastus, which contains a large number of type I muscle fibers, in each specimen (Fig. 8A), since the weight and the 300-fiber CSA of the soleus muscle, which includes numerous type I muscle fibers (Supplementary data), were decreased in the PPE 0.1 group. A significantly lower proportion of type I muscle fibers was observed in the ROI of the PPE 0.1 group than in the Control group (Fig. 8B and C). However, there were no significant differences in the proportion of type IIA, IID/X or IIB fibers among all of the groups. Lm showed a moderate correlation with the soleus muscle mass normalized to body weight, 300-fiber CSA of soleus, and proportion of type I muscle fibers in the intermediate vastus (Fig. 8D).

4. Discussion

This study was performed to establish a COPD/emphysema-related osteoporosis mouse model for elucidating the pathological mechanism of COPD/emphysema-related osteoporosis, and the following results were observed according to the purposes of this study. 1) PPE 0.025 U and PPE 0.1 U were the appropriate doses (Fig. 1 B–D) when we examined the elastase dose that induced emphysema without complications. Therefore, the bone and muscle data were compared among the PPE 0.1, PPE 0.025 and Control groups. 2) The BMD change rates from

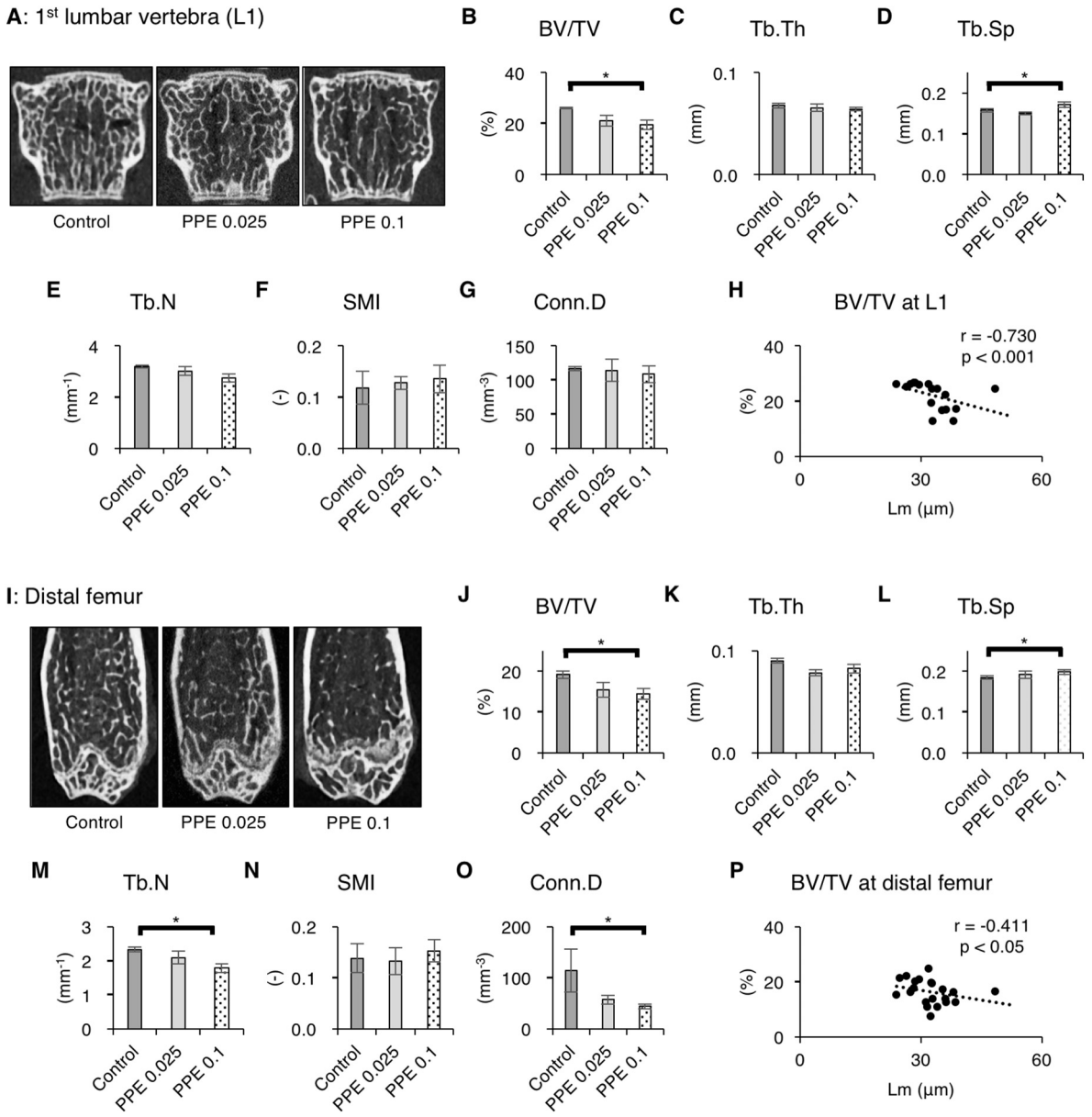

Fig. 3. Analysis of the trabecular microstructure by microcomputed tomography.
(A) Representative 3D imaging at the 1st lumbar vertebra (L1). The parameters of (B–G) the L1. (H) Relationship between the extent of emphysema and BV/TV at L1. (I) Representative 3D imaging at the distal femur. The parameters of (J–O) the distal femur. (P) Relationship between the extent of emphysema and BV/TV at the distal femur. Data are the mean ± SE (n = 7 in each group). *p < 0.05.

the upper thoracic vertebra (T4) to the lower lumbar vertebrae (L4) at weeks 4, 8, and 12 after a PPE administration showed significantly lower values in the PPE 0.1 group (Fig. 2A–E). The BMD measured by DXA of the extracted vertebrae in PPE 0.1 group was significantly lower than that in the Control group (Fig. 2F). The cancellous bone at both L1 and the femur scanned by μCT showed microstructural degradations (BV/TV, Tb.Sp, Tb.N, Conn.D, Fig. 3). Dynamic histomorphometry of the lumbar vertebrae and the proximal part of the tibiae showed significant declines in osteogenesis (OS/BS, MS/BS, MAR, BFR/BS), and a low value of plasma osteocalcin, which is a bone formation marker, was shown (Figs. 4–6). However, a significant decrease in soleus muscle weight in the PPE 0.1 group was observed (Fig. 7). The soleus muscle contains a large number of type I muscle fibers, and a significant decrease in type I muscle fibers was observed in the intermediate vastus, which similarly contains type I muscle fibers (Fig. 8B and C). Based on the above results, we will discuss below and verify whether this animal model will be established as a COPD/emphysema-related osteoporosis mouse model.

There are many reports on the reduction of BMD in patients with COPD, which are consistent with our mice data [2–6]. Regarding the bone metabolism dynamics of COPD-related osteoporosis, there is an opposing opinion [38] and one that supports our results (the value of plasma osteocalcin in elastase-induced emphysema mice was low), but there is no consensus view. The reasons for a lack of consensus on bone metabolism dynamics in COPD patients include the different subjects among studies and the possibility that several factors, such as gender, age and pneumonia, have also been involved. The gender and age of the mice in this study were selected to be male and middle-aged, respectively. Xiaomei et al. [39] demonstrated that the bone formation marker in elderly male COPD patients was significantly lower. When targeting middle-aged and elderly men, the bone metabolism dynamics are considered to be bone loss caused by impaired osteogenesis, which are consistent with the mice data obtained in this study.

Vertebral fractures in patients with COPD characteristically occur at

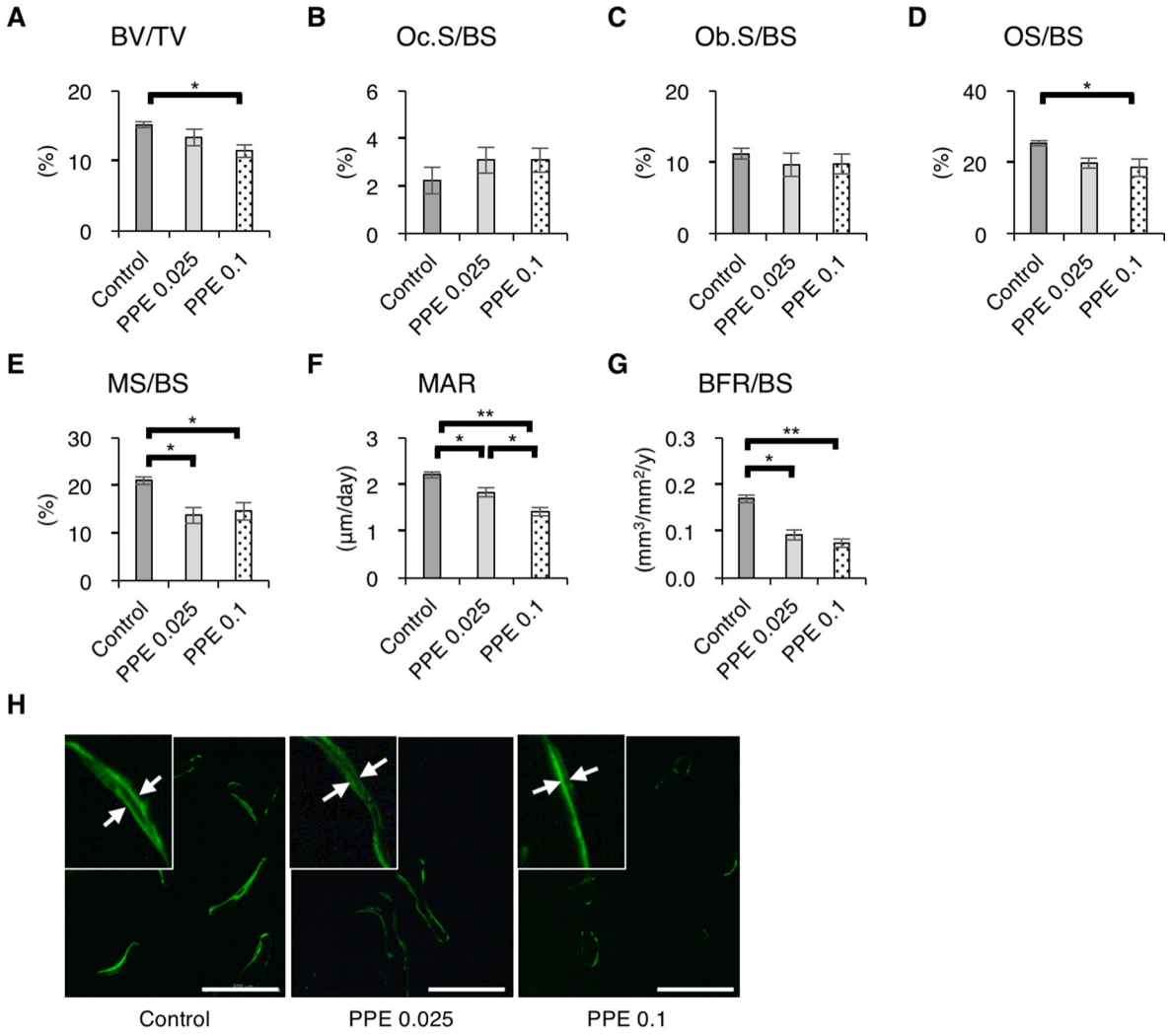

Fig. 4. Static and dynamic bone histomorphometry at the 1st–4th lumbar vertebrae.
(A) BV/TV, (B) Oc.S/BS, (C) Ob.S/BS, (D) OS/BS, (E) MS/BS, (F) MAR and (G) BFR/BS. Data are the mean ± SE (n = 6–7 in each group). *$p < 0.05$, **$p < 0.01$. (H) The fluorescence microscopy findings from the lumbar vertebrae, double-labeled by calcein. The width of the double-labeled area in the PPE 0.025 group was significantly narrower than in the Control group, and the width in the PPE 0.1 group was much narrower. Scale bar = 200 μm.

the thoracic vertebrae (T8–12) more often than the lumbar vertebrae [40]. Although we considered the possibility that the lower thoracic vertebrae might be accompanied by local bone fragility, the BMD change rates declined at almost all of the vertebrae (T4–L4) in the PPE 0.1 group in our study. Consistent with our results, BMD decline has been shown at almost every vertebra calculated by CT in patients with COPD [41]. Vertebral fractures of patients with COPD frequently occur in lower thoracic vertebrae (T8–12). For this reason, we believe that the lower thoracic vertebrae tend to be exposed to concentrated stress due to external factors (coughing and falling) and that fractures occur easily in patients with systemic bone fragility, as in COPD cases.

The cancellous bone loss of the PPE 0.1 group mice existed not only in the vertebrae but also in the femur. A previous report showed that the BMD of both the lumbar vertebrae and femur are decreased in patients with COPD [10]. In addition, COPD was noted in 47% of patients with hip fractures, and it is suggested that COPD is a risk factor of not only vertebral fractures but also hip fractures [42]. The values of the dynamic histomorphometric parameters (MAR, BFR/BS) in the PPE 0.1 group were significantly lower than those in the Control group. Since plasma osteocalcin, a bone formation marker, decreased without the elevation of the plasma TRACP-5b value, it was suggested that the COPD/emphysema-related osteoporosis is a low-turnover-type osteoporosis. In addition, hamsters with elastase-induced emphysema have been previously demonstrated to have impaired bone formation of cortical bone [43]. Therefore, it was suggested that pulmonary emphysema might be a factor that systemically induces the bone loss and reduction of osteogenic activity.

In the PPE 0.1 group, only the soleus muscle was decreased in weight among the muscles of the lower limbs. The soleus muscle contains a large number of type I muscle fibers (Supplementary data), and a significant decrease in type I muscle fibers was observed in the intermediate vastus, which similarly contains type I muscle fibers. The atrophy of type I muscle fibers has been reported in a systematic review of COPD cases [44]. Type I muscle fibers are mainly observed in the skeletal muscles responsible for endurance exercise and play a very important role in locomotion and posture maintenance against load or gravity. Studies aiming to elucidate the pathological mechanism of atrophy of type I muscle fibers associated with COPD/emphysema and the prevention of its onset may lead to beneficial effects on bones and motor function. We found that type II muscle fibers do not change even in mice with elastase-induced emphysema. One of the reasons is that 300-fiber CSA of gastrocnemius muscle composed of type II muscle fibers did not change at all. However, since the 300-fiber CSA of the soleus muscle (composed of Type I and Type IIA) was shown to decrease, Type IIA muscle fibers may be atrophied. Although the intermediate vastus was used as a substitute for the soleus in this study, it

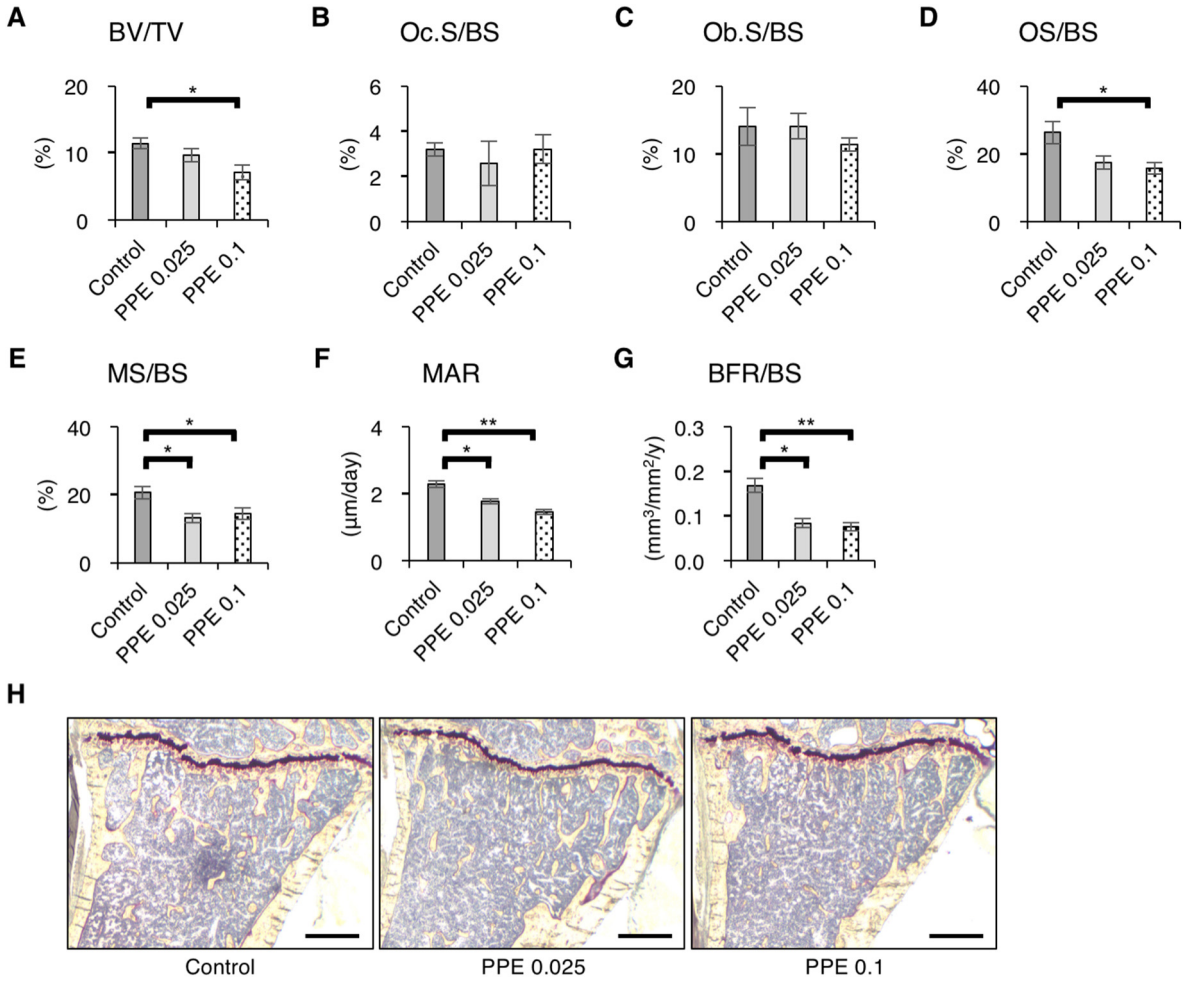

Fig. 5. Static and dynamic bone histomorphometry at the proximal tibia.
(A) BV/TV, (B) Oc.S/BS, (C) Ob.S/BS, (D) OS/BS, (E) MS/BS, (F) MAR and (G) BFR/BS. Data are the mean ± SE (n = 6–7 in each group). *p < 0.05, **p < 0.01. (H) The light microscopy findings at the proximal tibia. Trabecular bone at the proximal tibia in the PPE 0.1 group also decreased with the decline of osteogenic activity compared to that in the Control group. Scale bar = 500 μm.

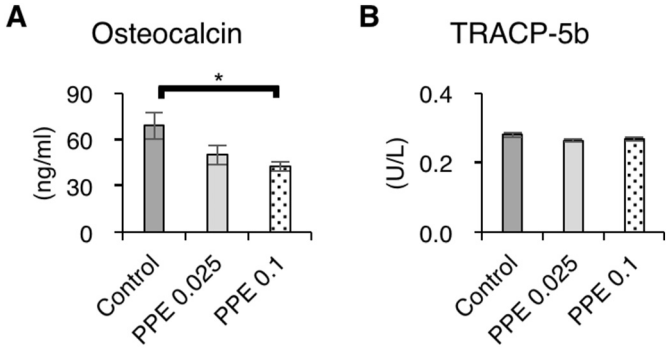

Fig. 6. Systemic chemical markers of bone metabolism.
The plasma levels of (A) osteocalcin and (B) TRACP-5b. Data are the mean ± SE (n = 6–7 in each group). *p < 0.05.

seems necessary to evaluate the muscle fibers of the soleus in the future.

Muscle atrophy can affect specific fiber types, involving predominantly type I or type II muscle fibers, and is frequently accompanied by a slow-to-fast or fast-to-slow fiber type shift. For example, muscle disuse, such as in a spinal cord injury, causes type I fiber atrophy with a slow-to-fast fiber type shift, whereas aging and cancer cachexia leads to preferential atrophy of type II fibers with a fast-to-slow fiber type shift [45]. The identification of the signaling pathways responsible for the differential response of muscles types and fiber types can lead to a better understanding of the pathogenesis of muscle wasting and to the design of therapeutic interventions appropriate for the specific disorders [45]. In general, the muscle fiber type shifting in COPD has been thought to be different from muscle atrophy due to aging, and the underlying mechanism is almost unknown. We plan to conduct further investigations using this mouse model in the future.

The limitations of this study are as follows. 1) Notably, the emphysema model used in this study is elastase inducible, and the endogenous elastase activity inhibitory effect varies depending on animals, strains, and individuals. Importantly, the same dose of elastase does not always induce similar pulmonary emphysema. 2) Animal activity was not evaluated in this study. In general, if activity declines, muscle fiber atrophy centering on type II muscle fibers occurs [46,47], and muscle mass and body weight decrease. Although there is concern about the decrease in momentum against an exercise load [25,48], we assumed that at least the basic activity level had not declined. 3) An elastase-induced model differs from human COPD in that it causes acute inflammation and promptly induces pulmonary emphysema. However, this model has many findings similar to human COPD and smoking exposure animal models, and it has been used as a COPD animal model. It would be necessary to examine the time course of lung destruction and inflammation and to determine whether or not these factors correlate with bone loss. However, we did not investigate this in the present study. If the effect of acute inflammation is a principal factor, BMD

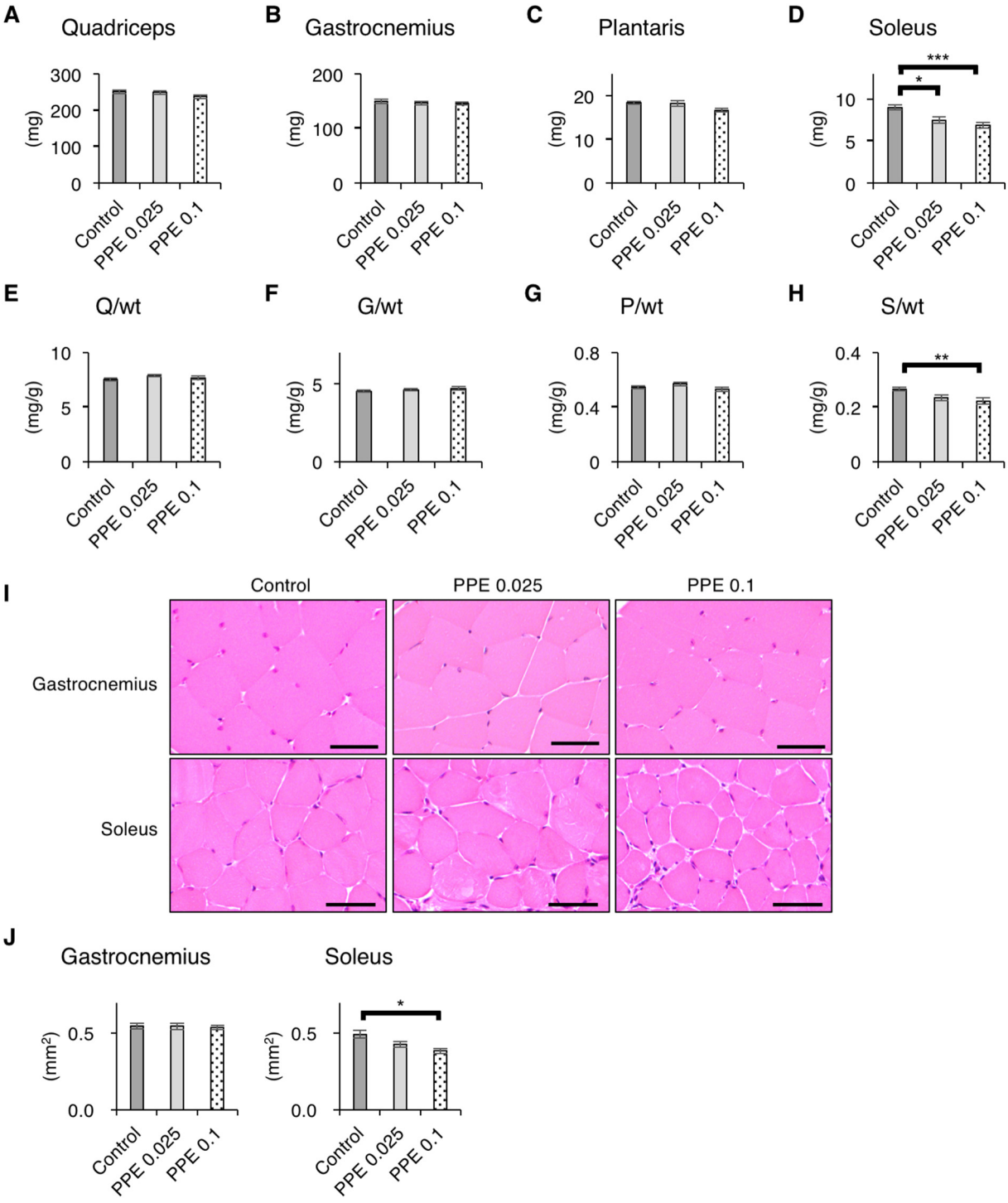

Fig. 7. Analysis of the lower limb muscles.
The weight of the (A) quadriceps, (B) gastrocnemius, (C) plantaris, and (D) soleus. The weight of the (E) quadriceps, (F) gastrocnemius, (G) plantaris, and (H) soleus normalized to body weight. Data are the mean ± SE (n = 14 in each group). *p < 0.05, **p < 0.01, ***p < 0.001. (I) The light microscopy findings and (J) cross sectional area (CSA) of 300 fibers in the gastrocnemius and soleus. Data are the mean ± SE (n = 7 in each group). Scale bar = 50 μm.

should gradually improve; however, the difference in the BMD change rate after week 4 from the Control group increased. Although the effects of acute inflammation cannot be completely eliminated, we believe that the bone loss and bone metabolism dynamics at week 12 after PPE administration reflect the effects of pulmonary emphysema.

Finally, even if these limitations are taken into consideration, we believe that these model mice will be accepted as a COPD/emphysema-related osteoporosis model.

5. Conclusions

The bone and muscle phenotypes in the mice with elastase-induced emphysema were highly similar to those previously reported in patients with COPD. We believe that the mice described in this experimental protocol will be accepted as a COPD/emphysema-related osteoporosis model.

Supplementary data to this article can be found online at https://

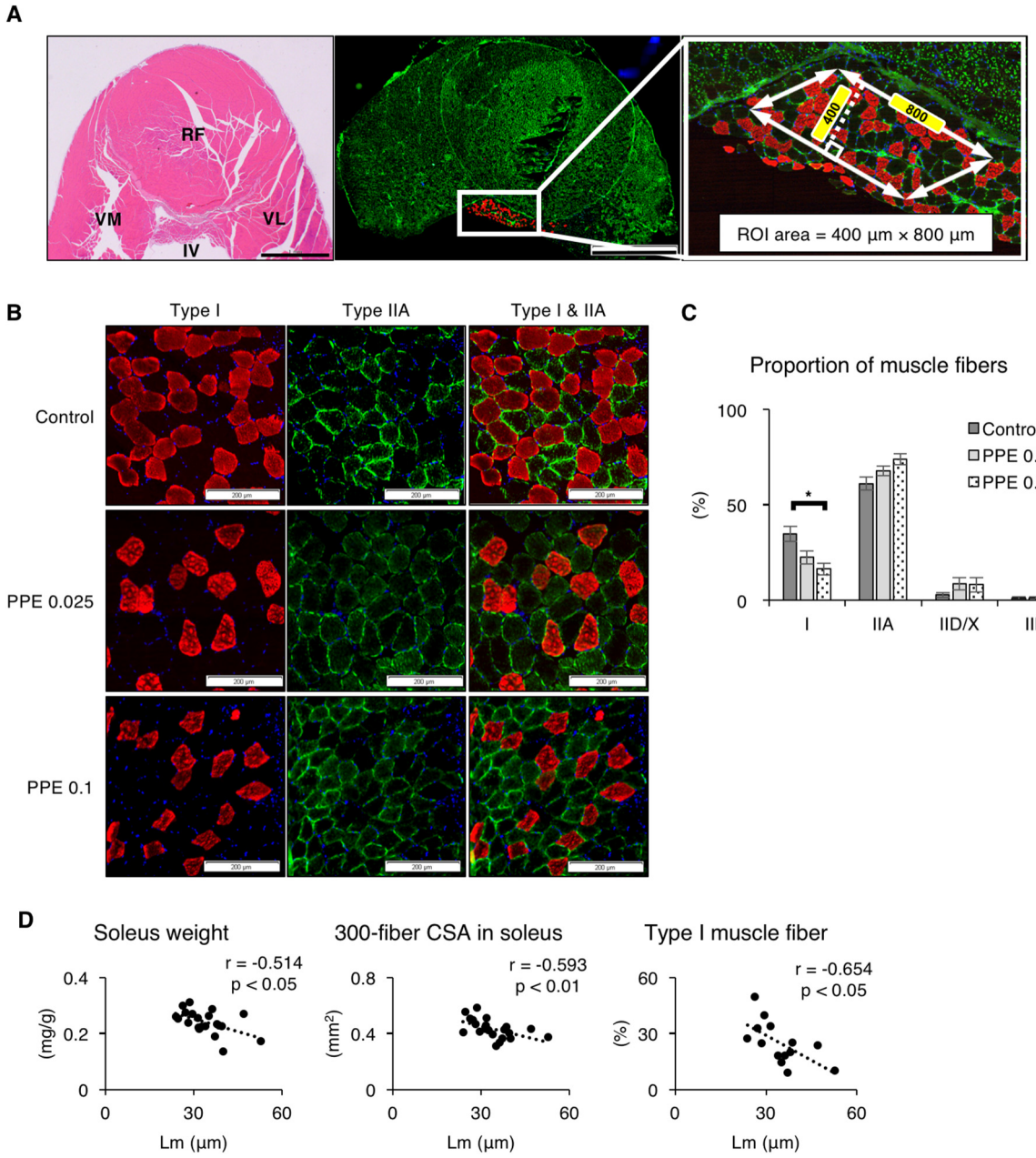

Fig. 8. Analysis of type I muscle fibers.
(A) Images of H&E staining (left panel), immunofluorescence staining (middle panel), and the ROI in the intermediate vastus (right panel). Scale bar = 1 mm. (B) Double-stained specimens of type I and type IIA muscle fibers. The atrophy of type I muscle fibers in the intermediate vastus was detected in the PPE 0.1 group. Scale bar = 200 μm. (C) The proportion of each fiber. Data are the mean ± SE (n = 5 in each group). (D) Relationship between the extent of emphysema and soleus mass normalized to body weight, 300-fiber CSA in soleus, or proportion of type I muscle fibers. *p < 0.05. RF, rectus femoris; VL, vastus lateralis; VM, vastus medialis; IV, intermediate vastus.

doi.org/10.1016/j.bone.2018.10.017.

Disclosures

None of the authors have conflicts of interest to disclose.

Acknowledgments

The authors greatly appreciate the technical assistance of Nao Terada (Department of Orthopaedic Surgery), Minako Nimura (Department of Orthopaedic Surgery) and Ryoko Maekado (Shared-Use Research Center) from the University of Occupational and Environmental Health. This work was supported, in part, by a Grant-in-Aid for Scientific Research (JSPS KAKENHI Grant Number JP 16H07390) and Japan Osteoporosis Society 2018 Research Encouragement Award.

References

[1] K.F. Rabe, B. Beghe, F. Luppi, L.M. Fabbri, Update in chronic obstructive pulmonary disease 2006, Am. J. Respir. Crit. Care Med. 175 (12) (2007) 1222–1232.
[2] D.D. Sin, J.P. Man, S.F. Man, The risk of osteoporosis in Caucasian men and women with obstructive airways disease, Am. J. Med. 114 (1) (2003) 10–14.
[3] A. Kjensli, P. Mowinckel, M.S. Ryg, J.A. Falch, Low bone mineral density is related to severity of chronic obstructive pulmonary disease, Bone 40 (2) (2007) 493–497.
[4] T.T. Dam, S. Harrison, H.A. Fink, J. Ramsdell, E. Barrett-Connor, Bone mineral density and fractures in older men with chronic obstructive pulmonary disease or asthma, Osteoporos. Int. 21 (8) (2010) 1341–1349.

[5] J.M. Duckers, B.A. Evans, W.D. Fraser, M.D. Stone, C.E. Bolton, D.J. Shale, Low bone mineral density in men with chronic obstructive pulmonary disease, Respir. Res. 12 (2011) 101.
[6] K. Schnell, C.O. Weiss, T. Lee, J.A. Krishnan, B. Leff, J.L. Wolff, et al., The prevalence of clinically-relevant comorbid conditions in patients with physician-diagnosed COPD: a cross-sectional study using data from NHANES 1999–2008, BMC Pulm. Med. 12 (2012) 26.
[7] S. Bernard, P. Leblanc, F. Whittom, G. Carrier, J. Jobin, R. Belleau, et al., Peripheral muscle weakness in patients with chronic obstructive pulmonary disease, Am. J. Respir. Crit. Care Med. 158 (2) (1998) 629–634.
[8] J.M. Seymour, M.A. Spruit, N.S. Hopkinson, S.A. Natanek, W.D. Man, A. Jackson, et al., The prevalence of quadriceps weakness in COPD and the relationship with disease severity, Eur. Respir. J. 36 (1) (2010) 81–88.
[9] R. Watanabe, T. Tanaka, K. Aita, M. Hagiya, T. Homma, K. Yokosuka, et al., Osteoporosis is highly prevalent in Japanese males with chronic obstructive pulmonary disease and is associated with deteriorated pulmonary function, J. Bone Miner. Metab. 33 (4) (2015) 392–400.
[10] A. Lehouck, S. Boonen, M. Decramer, W. Janssens, COPD, bone metabolism, and osteoporosis, Chest 139 (3) (2011) 648–657.
[11] L. Graat-Verboom, B.E. van den Borne, F.W. Smeenk, M.A. Spruit, E.F. Wouters, Osteoporosis in COPD outpatients based on bone mineral density and vertebral fractures, J. Bone Miner. Res. 26 (3) (2011) 561–568.
[12] C.S. Ryan, V.I. Petkov, R.A. Adler, Osteoporosis in men: the value of laboratory testing, Osteoporos. Int. 22 (6) (2011) 1845–1853.
[13] J.J. Atkinson, R.M. Senior, Matrix metalloproteinase-9 in lung remodeling, Am. J. Respir. Cell Mol. Biol. 28 (1) (2003) 12–24.
[14] V. Cottin, H. Nunes, P.Y. Brillet, P. Delaval, G. Devouassoux, I. Tillie-Leblond, et al., Combined pulmonary fibrosis and emphysema: a distinct underrecognised entity, Eur. Respir. J. 26 (4) (2005) 586–593.
[15] K. Ikezoe, T. Handa, K. Tanizawa, T. Kubo, T. Oguma, S. Hamada, et al., Bone mineral density in patients with idiopathic pulmonary fibrosis, Respir. Med. 109 (9) (2015) 1181–1187.
[16] K.D. Ward, R.C. Klesges, A meta-analysis of the effects of cigarette smoking on bone mineral density, Calcif. Tissue Int. 68 (5) (2001) 259–270.
[17] L. Graat-Verboom, E.F. Wouters, F.W. Smeenk, B.E. van den Borne, R. Lunde, M.A. Spruit, Current status of research on osteoporosis in COPD: a systematic review, Eur. Respir. J. 34 (1) (2009) 209–218.
[18] H. Kiyokawa, S. Muro, T. Oguma, S. Sato, N. Tanabe, T. Takahashi, et al., Impact of COPD exacerbations on osteoporosis assessed by chest CT scan, COPD 9 (3) (2012) 235–242.
[19] R.S. Weinstein, Clinical practice. Glucocorticoid-induced bone disease, N. Engl. J. Med. 365 (1) (2011) 62–70.
[20] C.E. Bolton, A.A. Ionescu, K.M. Shiels, R.J. Pettit, P.H. Edwards, M.D. Stone, et al., Associated loss of fat-free mass and bone mineral density in chronic obstructive pulmonary disease, Am. J. Respir. Crit. Care Med. 170 (12) (2004) 1286–1293.
[21] J.L. Wright, M. Cosio, A. Churg, Animal models of chronic obstructive pulmonary disease, Am. J. Phys. Lung Cell. Mol. Phys. 295 (1) (2008) L1–15.
[22] M. Sasaki, S. Chubachi, N. Kameyama, M. Sato, M. Haraguchi, M. Miyazaki, et al., Effects of long-term cigarette smoke exposure on bone metabolism, structure, and quality in a mouse model of emphysema, PLoS One 13 (1) (2018) e0191611.
[23] V. Ghorani, M.H. Boskabady, M.R. Khazdair, M. Kianmeher, Experimental animal models for COPD: a methodological review, Tob. Induc. Dis. 15 (2017) 25.
[24] N. Cielen, K. Maes, N. Heulens, T. Troosters, G. Carmeliet, W. Janssens, et al., Interaction between physical activity and smoking on lung, muscle, and bone in mice, Am. J. Respir. Cell Mol. Biol. 54 (5) (2016) 674–682.
[25] H. Yao, S. Chung, J.W. Hwang, S. Rajendrasozhan, I.K. Sundar, D.A. Dean, et al., SIRT1 protects against emphysema via FOXO3-mediated reduction of premature senescence in mice, J. Clin. Invest. 122 (6) (2012) 2032–2045.
[26] S. Kobayashi, R. Fujinawa, F. Ota, S. Kobayashi, T. Angata, M. Ueno, et al., A single dose of lipopolysaccharide into mice with emphysema mimics human chronic obstructive pulmonary disease exacerbation as assessed by micro-computed tomography, Am. J. Respir. Cell Mol. Biol. 49 (6) (2013) 971–977.
[27] J.D. Lourenço, L.P. Neves, C.R. Olivo, A. Duran, F.M. Almeida, P.M.M. Arantes, et al., A treatment with a protease inhibitor recombinant from the cattle tick (*Rhipicephalus Boophilus microplus*) ameliorates emphysema in mice, PLoS One 9 (6) (2014) 1–9.
[28] S. Ito, E.P. Ingenito, K.K. Brewer, L.D. Black, H. Parameswaran, K.R. Lutchen, et al., Mechanics, nonlinearity, and failure strength of lung tissue in a mouse model of emphysema: possible role of collagen remodeling, J. Appl. Physiol. 98 (2) (2005) 503–511 (1985).
[29] L.R. Margraf, J.F.J. Tomashefski, M.C. Bruce, B.B. Dahms, Morphometric analysis of the lung in bronchopulmonary dysplasia, Am. Rev. Respir. Dis. 143 (2) (1991) 391–400.
[30] T. Tajima, K. Menuki, K.F. Okuma, M. Tsukamoto, H. Fukuda, Y. Okada, et al., Cortical bone loss due to skeletal unloading in aldehyde dehydrogenase 2 gene knockout mice is associated with decreased PTH receptor expression in osteocytes, Bone 110 (2018) 254–266.
[31] K.F. Okuma, K. Menuki, M. Tsukamoto, T. Tajima, H. Fukuda, Y. Okada, et al., Disruption of the aldehyde dehydrogenase 2 gene results in no increase in trabecular bone mass due to skeletal loading in association with impaired cell cycle regulation through p21 expression in the bone marrow cells of mice, Calcif. Tissue Int. 101 (3) (2017) 328–340.
[32] M. Tsukamoto, K. Menuki, T. Murai, A. Hatakeyama, S. Takada, K. Furukawa, et al., Elcatonin prevents bone loss caused by skeletal unloading by inhibiting preosteoclast fusion through the unloading-induced high expression of calcitonin receptors in bone marrow cells, Bone 85 (2016) 70–80.
[33] K.Y. Wang, S. Yamada, H. Izumi, M. Tsukamoto, T. Nakashima, T. Tasaki, et al., Critical in vivo roles of WNT10A in wound healing by regulating collagen expression/synthesis in WNT10A-deficient mice, PLoS One 13 (3) (2018) e0195156.
[34] M.L. Bouxsein, S.K. Boyd, B.A. Christiansen, R.E. Guldberg, K.J. Jepsen, R. Muller, Guidelines for assessment of bone microstructure in rodents using micro-computed tomography, J. Bone Miner. Res. 25 (7) (2010) 1468–1486.
[35] A.M. Parfitt, M.K. Drezner, F.H. Glorieux, J.A. Kanis, H. Malluche, P.J. Meunier, et al., Bone histomorphometry: standardization of nomenclature, symbols, and units. Report of the ASBMR Histomorphometry Nomenclature Committee, J. Bone Miner. Res. 2 (6) (1987) 595–610.
[36] D.W. Dempster, J.E. Compston, M.K. Drezner, F.H. Glorieux, J.A. Kanis, H. Malluche, et al., Standardized nomenclature, symbols, and units for bone histomorphometry: a 2012 update of the report of the ASBMR Histomorphometry Nomenclature Committee, J. Bone Miner. Res. 28 (1) (2013) 2–17.
[37] Y. Jeong, S.M. Carleton, B.A. Gentry, X. Yao, J.A. Ferreira, D.J. Salamango, et al., Hindlimb skeletal muscle function and skeletal quality and strength in +/G610C mice with and without weight-bearing exercise, J. Bone Miner. Res. 30 (10) (2015) 1874–1886.
[38] I. Stanojkovic, J. Kotur-Stevuljevic, S. Spasic, B. Milenkovic, T. Vujic, A. Stefanovic, et al., Relationship between bone resorption, oxidative stress and inflammation in severe COPD exacerbation, Clin. Biochem. 46 (16–17) (2013) 1678–1682.
[39] W. Xiaomei, X. Hang, L. Lingling, L. Xuejun, Bone metabolism status and associated risk factors in elderly patients with chronic obstructive pulmonary disease (COPD), Cell Biochem. Biophys. 70 (1) (2014) 129–134.
[40] L. Graat-Verboom, F.W. Smeenk, B.E. van den Borne, M.A. Spruit, A.B. Donkers-van Rossum, R.P. Aarts, et al., Risk factors for osteoporosis in Caucasian patients with moderate chronic obstructive pulmonary disease: a case control study, Bone 50 (6) (2012) 1234–1239.
[41] T. Ohara, T. Hirai, S. Muro, A. Haruna, K. Terada, D. Kinose, et al., Relationship between pulmonary emphysema and osteoporosis assessed by CT in patients with COPD, Chest 134 (6) (2008) 1244–1249.
[42] E.A. Regan, T.A. Radcliff, W.G. Henderson, D.C. Cowper Ripley, M.L. Maciejewski, W.B. Vogel, et al., Improving hip fractures outcomes for COPD patients, COPD 10 (1) (2013) 11–19.
[43] J.E. Shea, S.C. Miller, D.C. Poole, J.P. Mattson, Cortical bone dynamics, strength, and densitometry after induction of emphysema in hamsters, J. Appl. Physiol. 95 (2) (2003) 631–634 (1985).
[44] H.R. Gosker, M.P. Zeegers, E.F. Wouters, A.M. Schols, Muscle fibre type shifting in the vastus lateralis of patients with COPD is associated with disease severity: a systematic review and meta-analysis, Thorax 62 (11) (2007) 944–949.
[45] S. Ciciliot, A.C. Rossi, K.A. Dyar, B. Blaauw, S. Schiaffino, Muscle type and fiber type specificity in muscle wasting, Int. J. Biochem. Cell Biol. 45 (10) (2013) 2191–2199.
[46] C.B. Mantilla, S.M. Greising, W.Z. Zhan, Y.B. Seven, G.C. Sieck, Prolonged C2 spinal hemisection-induced inactivity reduces diaphragm muscle specific force with modest, selective atrophy of type IIx and/or IIb fibers, J. Appl. Physiol. 114 (3) (2013) 380–386 (1985).
[47] C.R. Lamboley, V.L. Wyckelsma, B.D. Perry, M.J. McKenna, G.D. Lamb, Effect of 23-day muscle disuse on sarcoplasmic reticulum Ca^{2+} properties and contractility in human type I and type II skeletal muscle fibers, J. Appl. Physiol. 121 (2) (2016) 483–492 (1985).
[48] L. Luthje, T. Raupach, H. Michels, B. Unsold, G. Hasenfuss, H. Kogler, et al., Exercise intolerance and systemic manifestations of pulmonary emphysema in a mouse model, Respir. Res. 10 (2009) 7.